Proceedings of ASME Turbo Expo 2011
GT2011
June 6-10, 2011, Vancouver, British Columbia, Canada

GT2011-46698

A STATISTICAL CHARACTERIZATION OF THE EFFECTS OF MISTUNING IN MULTI-STAGE BLADED DISKS

Kiran X. D'Souza
Department of Mechanical Engineering
University of Michigan
Ann Arbor, Michigan, 48109-2125
Email: kdsouza@umich.edu

Bogdan I. Epureanu*
Department of Mechanical Engineering
University of Michigan
Ann Arbor, Michigan, 48109-2125
Email: epureanu@umich.edu

ABSTRACT

A great deal of research has been conducted on the effects of small random variations in structural properties, known as mistuning, in single stage bladed disks. Due to the inherent randomness of mistuning and the large dimensionality of the models of industrial bladed disks, a reduced order modeling approach is required to understand the effects of mistuning on a particular bladed disk design. Component mode mistuning (CMM) is an efficient compact reduced order modeling method that was developed to handle this challenge in single stage bladed disks. In general, there are multiple stages in bladed disk assemblies, and it has been demonstrated that for certain frequency ranges accurate modeling of the entire bladed disk assembly is required because multi-stage modes exist. In this work, a statistical characterization of structural mistuning in multi-stage bladed disks is carried out. The results were obtained using CMM combined with a multi-stage modeling approach previously developed. In addition to the statistical characterization, a new efficient classification method is detailed for characterizing the properties of a mode. Also, the effects of structural mistuning on the characterization of the mode is explored.

NOMENCLATURE

CMM	Component mode mistuning
CMS	Component mode synthesis
DOF	Degree of freedom
FEM	Finite element model
MAC	Modal assurance criterion
ROM	Reduced order model
b	Subscript that denotes inter-stage boundary
h	Superscript that denotes the harmonic number
i	Subscript that denotes the interior of the stage
j	Subscript that denotes the stage number
$\tilde{\mathbf{p}}(t)$	Generalized reduced coordinates
$\mathbf{q}$	Cantilever blade modal participation factor
r	Subscript that indicates radial line segment
$\mathbf{u}^h_{c,s}$	Vector of Fourier coefficients where subscript c or s indicates cosine or sine function
$\mathbf{x}(t)$	Nodal displacement on all nodes of all sectors of one stage
$\mathbf{x}_n$	Displacement of nodes on the n^{th} sector
$\mathbf{z}^h_{jc,s}$	Vector of Fourier coefficients where subscript c or s indicates cosine or sine function
B	Number of basis functions used for the Fourier expansion along the inter-stage boundary
E_{ij}	Energy of the i^{th} mode contained in the j^{th} stage
ER_{ij}	Strain energy ratio of the j^{th} stage for the i^{th} mode
$\mathbf{F}_{n,m}$	Fourier matrix of size $n \times m$
$\mathbf{I}_n$	Identity matrix of size $n \times n$
$\mathbf{K}$	Multi-stage reduced order stiffness matrix
$\mathbf{M}$	Multi-stage reduced order mass matrix
$M_{1,2}$	Multi-stage mode
M_{S1}	Stage 1 - multi-stage mode
M_{S2}	Stage 2 - multi-stage mode
$M_{S1,S2}$	Multi-stage - double single stage mode
MAC_{ij}	MAC number of the i^{th} mode of the j^{th} stage

*Address all correspondence to this author.

N	Number of sectors on a stage
N_b	Number of DOFs along the inter-stage boundary
N_S	Number of DOFs in a sector
R	Set of retained cantilever blade modes
$S1$	Stage 1 - single stage mode
$S2$	Stage 2 - single stage mode
Z_j	Number of radial line segments per sector of the j^{th} stage
κ_j	Reduced order stiffness matrix of the j^{th} stage
$\delta\lambda^{CB}$	Difference in the tuned and mistuned cantilever blade eigenvalues
$\boldsymbol{\Lambda}_j$	Diagonal matrix of tuned eigenvalues of the j^{th} stage
$\boldsymbol{\Phi}_i^h$	Truncated set of fixed-interface normal modes for the h^{th} harmonic
$\boldsymbol{\Psi}_i^h$	Constraint modes for the h^{th} harmonic

INTRODUCTION

A significant amount of research has been conducted on the vibration response of bladed disks. An extensive review of this research was conducted by Castanier and Pierre [1]. Early work in the area of vibration of bladed disks focused on simple lumped parameter models of single stage bladed disks [2–6]. These models were developed in part to understand the effects of mistuning. Mistuning is a random variation in the structural properties of a system, which can be caused by manufacturing tolerances and/or operational wear. Even small levels of mistuning can lead to a localization in the vibration energy to a few blades in the disk, and this localization can lead to a dramatic increase in the amplitude of the force response of these blades. While these simple lumped parameter models were useful in providing a qualitative understanding of certain features of the system such as mistuning, more accurate finite element models (FEMs) of the system were needed to obtain quantitative results. Due to the size of these FEMs, reduced order models (ROMs) of the system were constructed to conduct statistical analyses on these systems.

Early ROMs used component mode synthesis [7, 8] (CMS), which breaks the systems into components for faster analysis, and combines them at the interface using a fixed-interface, free-interface or hybrid method. Early work using free-interface CMS [9] was conducted by Irretier [10] and Zheng and Wang [11] who found significant savings in computational time relative to the parent FEMs. Eventually, powerful ROMs were developed that have a size of the order of the number of blades in the system yet retain high accuracy over a given frequency range. Yang and Griffin [12] had the first such approach called the subset of nominal modes method. This method used the fact, that when the mistuning is small, the tuned system modes provide an excellent basis for the vibration of the mistuned system. Later, Lim et al. [13] introduced a method called component mode mistuning (CMM), which uses both tuned system modes and blade component modes to construct ROMs. This method handles various types of mistuning in a systematic manner by modeling the mistuning in the blade alone using cantilevered blade modes.

While a great deal of research has been done on the vibration response of single stage bladed disks, far less has been done on multi-stage bladed disk systems. Sinha [14] conducted Monte Carlo simulations on a lumped parameter model of mistuned multi-stage systems to simulate the overall dynamics of multi-stage systems, but did not discuss its applicability to multi-stage systems with realistic geometry for industrial models. An investigation of FEMs of multi-stage bladed disks with blade mistuning was conducted by Bladh et al. [15]. It was shown that multi-stage effects due to the inter-stage coupling can occur when the frequency range of interest pass *veering regions*, where the motion of the disk is dominant. Additionally, it was pointed out that, when each stage has a different number of blades, mistuning is inherent in multi-stage systems due to the inter-stage coupling. Song et al. [16] created a novel reduced order modeling technique for multi-stage systems, and then united it with CMM to efficiently handle mistuning in multi-stage systems [17]. The approach was also used for parameter identification in multi-stage systems [18] and its applicability to structural health monitoring monitoring was explored [19]. Laxalde et al. [20, 21] proposed a method similar in concept to Song [19], and applied the method for modal analysis and forced response calculations for multi-stage industrial bladed disks. Additionally, there has been recent work on multi-stage effects induced by modeling the coupling between flexible shafts and rotors [22–26].

In this work new characteristics of multi-stage systems are explored. In particular, a statistical characterization of structural mistuning in multi-stage bladed disks is carried out. The results were obtained using CMM [13] combined with a new multi-stage modeling approach developed by D'Souza et al. [27], which is based on Song et al. [16]; however, it only requires the use of full single sector models of each stage (i.e. the multi-stage model is constructed in the reduced order space only). In addition to the statistical characterization, a new efficient classification method is detailed for characterizing modes of multi-stage bladed disk systems. Additionally, the effects of structural mistuning on the characterization of the modes is explored.

METHODOLOGY

In this section the modeling methodology is briefly reviewed, and a new classification method is described. The challenge associated with modeling multi-stage systems is caused by the fact that even if each stage is cyclically symmetric the entire multi-stage system is not (when the number of sectors in each stage is different). Song [19] successfully overcame this challenge by projecting the motion of the interface onto a set of Fourier basis functions and then enforcing compatibility. The major drawback associated with his formulation was that full multi-stage modes were needed when including small blade to blade mistuning. That requires the explicit formulation and analysis of the full order FEM. Recently, D'Souza et al. [27] proposed a new method to tackle multi-stage systems that can handle a combination of cyclic stages (this includes stages with small mistuning modeled with CMM) and non-cyclic stages (stages including cracks, large mistuning, etc.) by performing only analyses on individual stages (thus completely eliminating the need to form and analyze the full order FEM). This work closely follows the methodology presented in D'Souza et al. [27], but here all the stages are considered to have only mistuning. The following contains a brief review of the method presented in D'Souza et al. [27] and Song [19]. Next, a new classification scheme for modes of a multi-stage system is presented.

Multi-Stage ROMs from Cyclic Stages

A significant benefit of dealing with cyclic stages is that the analysis can be performed on sectors (and double sectors) instead of the full stage model, thus greatly reducing the computational cost. Let $\mathbf{x}(t)$ be the nodal displacement on all nodes of all sectors of one stage. $\mathbf{x}(t)$ can be partitioned such that it is ordered based on sectors, i.e. $\mathbf{x} = [\mathbf{x}_1^{\mathrm{T}}, \ldots, \mathbf{x}_N^{\mathrm{T}}]^{\mathrm{T}}$, where N is the number of sectors in the stage. The motion of the n^{th} sector can be described by the following Fourier series [28]

$$\begin{aligned}\mathbf{x}_n = \; & \frac{1}{\sqrt{N}}\mathbf{u}^0 + \sqrt{\frac{2}{N}}\sum_{h=1}^{\tilde{N}-1}\left(\mathbf{u}_c^h \cos(n-1)\phi_h + \mathbf{u}_s^h \sin(n-1)\phi_h\right) \\ & + \frac{1}{\sqrt{N}}(-1)^{n-1}\mathbf{u}^{\tilde{N}},\end{aligned} \tag{1}$$

where $\mathbf{u}$ denotes a vector of Fourier coefficients with subscripts c and s denoting cosine and sine components, $\phi_h = 2\pi h/N$, and $\tilde{N} = N/2$ if N is even or $\tilde{N} = (N-1)/2$ if N is odd. Note that the last term in Eqn. (1) does not exist if N is odd. Grouping the Fourier coefficients in matrix form $\tilde{\mathbf{u}} = [(\mathbf{u}^0)^{\mathrm{T}}, (\mathbf{u}_c^h)^{\mathrm{T}}, (\mathbf{u}_s^h)^{\mathrm{T}}, \ldots, (\mathbf{u}^{\tilde{N}})^{\mathrm{T}}]^{\mathrm{T}}$, the physical coordinates can be related by the following linear map

$$\mathbf{x}(t) = (\mathbf{F}_{N,N} \otimes \mathbf{I}_{N_s})\tilde{\mathbf{u}}(t), \tag{2}$$

where N_s is the number of degrees of freedom (DOFs) in a sector and $\mathbf{F}_{N,N}$ is an $N \times N$ Fourier matrix.

A cyclic Craig-Bampton method developed by Bladh et al. [29] can be applied to the displacement field to obtain

$$\tilde{\mathbf{u}}(t) \simeq \mathbf{\Phi}_{\mathcal{CB}}\, \tilde{\mathbf{p}}(t), \tag{3}$$

where $\mathbf{\Phi}_{\mathcal{CB}} = \underset{h=0,\ldots,\tilde{N}}{\mathrm{bdiag}} \begin{pmatrix} \mathbf{I}_{N_b} & \mathbf{0} \\ \mathbf{\Psi}_i^h & \mathbf{\Phi}_i^h \end{pmatrix}$, with $\underset{h=0,\ldots,\tilde{N}}{\mathrm{bdiag}}(\cdot)$ designating a block-diagonal matrix with the argument being the h^{th} block of the overall block-diagonal matrix. The matrix $[\mathbf{I}_{N_b}^{\mathrm{T}}, (\mathbf{\Psi}_i^h)^{\mathrm{T}}]^{\mathrm{T}}$ contains the constraint modes for the h^{th} harmonic, b indicates the inter-stage boundary, i denotes the interior of the stage, and N_b is the number of DOF along the inter-stage boundary of a single sector. A constraint mode for a stage is computed as the static deformation of the interior of the stage when a unit displacement is applied to one DOF along the boundary (and the rest of the boundary DOFs are fixed). The matrix $\mathbf{\Phi}_i^h$ is a truncated set of fixed-interface normal modes of the entire stage with all the boundary DOFs fixed. Finally, $\tilde{\mathbf{p}}(t)$ is the generalized reduced coordinates, where the size of $\tilde{\mathbf{p}}(t)$ is much less than that of $\tilde{\mathbf{u}}(t)$. Combining Eqn. (2) and Eqn. (3) yields

$$\mathbf{x}(t) \simeq (\mathbf{F}_{N,N} \otimes \mathbf{I}_{N_s})\mathbf{\Phi}_{\mathcal{CB}}\, \tilde{\mathbf{p}}(t). \tag{4}$$

It can be noted that the motion along the inter-stage boundary is

$$\mathbf{x}_b(t) = (\mathbf{F}_{N,N} \otimes \mathbf{I}_{N_b})\tilde{\mathbf{u}}_b(t). \tag{5}$$

After creating a ROM for each stage, the ROMs must be coupled. Consider the case where two stages are being coupled with the first having N_1 sectors and the second having N_2 sectors. The inter-stage boundary DOF can then be partitioned as $\mathbf{x}_{b_j} = [\mathbf{x}_{b_{j1}}^{\mathrm{T}}, \ldots, \mathbf{x}_{b_{jN_j}}^{\mathrm{T}}]^{\mathrm{T}}$, where j denotes the stage (i.e. $j = 1$ or 2). It is assumed that groups of nodes are aligned so that they have the same angle in a cylindrical coordinate system aligned with the axis of the multi-stage system. These groups of nodes are referred to as radial line segments, and Z_j of them exist in each sector of the j^{th} stage. Therefore, stage 1 has N_1Z_1 radial line segments, and stage 2 has N_2Z_2 radial line segments. The number of DOFs per radial line segment is given by N_{rj}. Figure 1 is a schematic of the radial line segments along the inter-stage boundary. Note that $\mathbf{x}_{b_j}$ can be partitioned as

$$\mathbf{x}_{b_j} = \begin{bmatrix} \mathbf{x}_{r_{j1}} \\ \vdots \\ \mathbf{x}_{r_{j(N_jZ_j)}} \end{bmatrix}, \tag{6}$$

where subscript r stands for the radial line segment and $\mathbf{x}_{b_{ji}}$ contains $\mathbf{x}_{r_{jk}}$ for $1 + (i-1)Z_j \leqslant k \leqslant iZ_j$.

Next, the motion of the k^{th} radial line segment is approximated by the following truncated Fourier series

$$\begin{aligned}\mathbf{x}_{r_{jk}} \simeq \; & \frac{1}{\sqrt{B}}\mathbf{z}_j^0 + \sqrt{\frac{2}{B}}\sum_{h=1}^{P-1}\left(\mathbf{z}_{jc}^h \cos(k-1)\theta_{h_j} + \mathbf{z}_{js}^h \sin(k-1)\theta_{h_j}\right) \\ & + \frac{1}{\sqrt{B}}(-1)^{k-1}\mathbf{z}_j^P,\end{aligned} \tag{7}$$

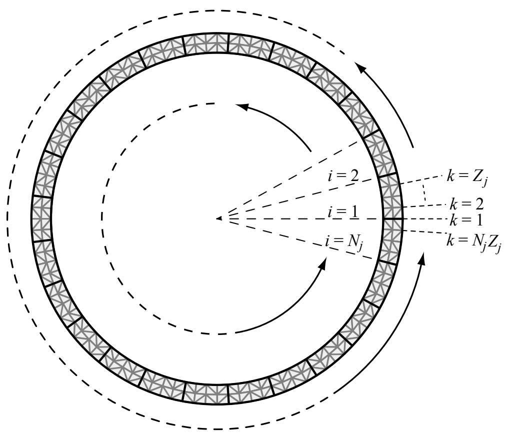

FIGURE 1. INTER-STAGE BOUNDARY (b-PARTITION) FOR A CYCLIC STAGE (i DENOTES A SECTOR, k DENOTES A RADIAL LINE SEGMENT).

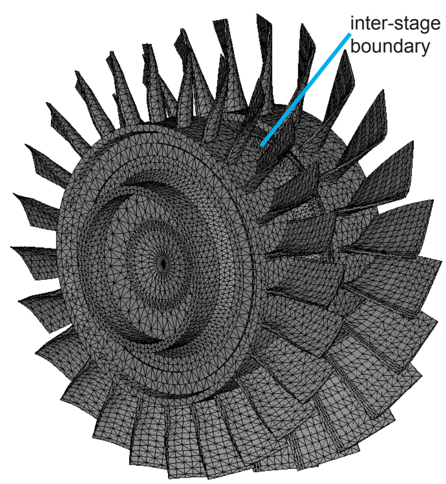

FIGURE 2. MULTI-STAGE TURBOMACHINERY ROTOR.

where $\theta_{h_j} \triangleq 2\pi h/(N_j Z_j)$, $\mathbf{z}$ represents the Fourier coefficients with superscript denoting the harmonic number, and subscripts c and s corresponding to a cosine or sine term, and B is the number of basis functions used for the Fourier expansion. Note that if B is even $P = B/2$, while if B is odd $P = (B-1)/2$ and the last term in Eqn. (7) does not exist. Combining Eqn. (6) and Eqn. (7) in matrix form gives

$$\mathbf{x}_{b_j} = \begin{bmatrix} \mathbf{x}_{r_{j1}} \\ \vdots \\ \mathbf{x}_{r_{jN_jZ_j}}, \end{bmatrix} \simeq \left(\mathbf{F}_{N_jZ_j,B} \otimes \mathbf{I}_{N_{rj}}\right)\tilde{\mathbf{z}}_j, \tag{8}$$

where $\mathbf{F}_{N_jZ_j,B}$ is a $N_jZ_j \times B$ Fourier matrix, and $\tilde{\mathbf{z}}_j = [(\mathbf{z}_j^0)^{\mathrm{T}}, (\mathbf{z}_{jc}^h)^{\mathrm{T}}, (\mathbf{z}_{js}^h)^{\mathrm{T}}, \ldots, (\mathbf{z}_j^P)^{\mathrm{T}}]^{\mathrm{T}}$. Inverting Eqn. (5) and combining it with Eqn. (8) yields

$$\tilde{\mathbf{u}}_{b_j}(t) \simeq \left(\mathbf{F}_{N_j,N_j} \otimes \mathbf{I}_{N_{b_j}}\right)^{\mathrm{T}} \left(\mathbf{F}_{N_jZ_j,B} \otimes \mathbf{I}_{N_{jr}}\right)\tilde{\mathbf{z}}_j. \tag{9}$$

The final step in the reduced order modeling process is to enforce geometric compatibility along the inter-stage boundary, i.e. $\tilde{\mathbf{z}}_1 = \tilde{\mathbf{z}}_2$. The enforcement of the compatibility conditions is approximate, however, the compatibility conditions are well posed [19] as long as enough Fourier coefficients B are used.

Mistuning can be incorporated into each stage with CMM by using a method detailed by Lim et al. [13]. In particular, for stiffness mistuning only, the reduced order stiffness matrix κ_j for the j^{th} stage can be written as

$$\kappa_j = \mathbf{\Lambda}_j + \sum_{n=1}^{N_j} \mathbf{q}_{j,n}^T \operatorname*{diag}_{r\in R}(\delta\lambda_{r,n,j}^{CB})\mathbf{q}_{j,n}, \tag{10}$$

where $\mathbf{\Lambda}$ is a matrix of tuned eigenvalues, $\mathbf{q}_{j,n}$ are modal partipation factors, $\delta\lambda_{r,n,j}^{CB}$ is the difference in the r^{th} tuned and mistuned cantilevered blade eigenvalues for sector n of stage j, and R is a set of retained cantilever blade modes.

Classification of Multi-Stage Modes

In this section a new classification scheme for multi-stage modes is discussed to better understand the effects of mistuning and the effects of inter-stage coupling in multi-stage systems. Two factors are used to classify the modes of a multi-stage system. The first factor is the strain energy distribution. The strain energy E of the i^{th} mode of an entire multi-stage system can be calculated very easily and effectively in the ROM coordinates as $E_i = \phi_i^{\mathrm{T}}\mathbf{K}\phi_i$, where $\mathbf{K}$ is the multi-stage reduced order stiffness matrix, and ϕ_i is the i^{th} mass normalized eigenvector of the multi-stage system. A detailed derivation of the reduced order mass and stiffness matrix can be found in previous works [16,27]. The corresponding energy in the j^{th} stage is given by $E_{ij} = \phi_{ij}^{\mathrm{T}}\mathbf{K}_j\phi_{ij}$, where $\mathbf{K}_j$ is the stiffness matrix for the j^{th} stage, and ϕ_{ij} is the portion of ϕ_i that corresponds to the j^{th} stage. The strain energy ratio for the i^{th} mode of stage 1 in a two stage system is given by

$$ER_{i1} = \frac{E_{i1}}{E_{i1} + E_{i2}}, \tag{11}$$

while for stage 2 it is

$$ER_{i2} = \frac{E_{i2}}{E_{i1} + E_{i2}}. \tag{12}$$

Mode Classification	Energy Distribution	Modal Alignment	Symbol
Stage 1 - single stage mode ($S1$)	$ER_1 > 0.9$	$MAC_1 > 0.9$	△
Stage 1 - multi-stage mode (M_{S1})	$ER_1 > 0.9$	$MAC_1 < 0.9$	▲
Stage 2 - single stage mode ($S2$)	$ER_2 > 0.9$	$MAC_2 > 0.9$	○
Stage 2 - multi-stage mode (M_{S2})	$ER_2 > 0.9$	$MAC_2 < 0.9$	●
Multi-stage - double single stage mode ($M_{S1,S2}$)	$ER_1 < 0.9$ AND $ER_2 < 0.9$	$MAC_1 > 0.9$ AND $MAC_2 > 0.9$	□
Mult-stage mode ($M_{1,2}$)	$ER_1 < 0.9$ AND $ER_2 < 0.9$	$MAC_1 < 0.9$ OR $MAC_2 < 0.9$	■

TABLE 1. CLASSIFICATION OF SIX TYPES OF MODES USING THE ENERGY DISTRIBUTION AND MODAL ALIGNMENT.

The two ratios ER_{i1} and ER_{i2} reflect the fractions of strain energy contained in each of the two stages.

The second factor used for classifying the modes of a multi-stage system is a form of the modal assurance criterion (MAC) number. The MAC number is a quantitative measure of the alignment of two modes. If the modes are parallel, the MAC number is one, and if the modes are orthogonal, the MAC number is zero. In this work, a variant of the MAC is used. Specifically, MAC_{ij} corresponds to the MAC number of the i^{th} mode of the j^{th} stage, and it is defined as

$$MAC_{ij} = \max_{k \in n_j} \sqrt{\frac{(\phi_{ij}^{\mathrm{T}} \mathbf{M}_j \varphi_{kj})^2}{|\phi_{ij}^{\mathrm{T}} \mathbf{M}_j \phi_{ij}| \, |\varphi_{kj}^{\mathrm{T}} \mathbf{M}_j \varphi_{kj}|}}, \tag{13}$$

where $\mathbf{M}_j$ is the mass matrix of the j^{th} stage, φ_{kj} is the k^{th} *single stage* mode from the j^{th} stage, and n_j is the set of *single stage* modes within the ROM of the j^{th} stage that are within a particular frequency range. This frequency range is related to the i^{th} multi-stage frequency ω_i and the k^{th} single stage frequency ω_{kj} of stage j. The criteria is that the frequency of the single stage mode must be within a given tolerance ε of the multi-stage mode for the single stage and multi-stage modes to be compared, i.e.

$$\varepsilon \geq \frac{|\omega_i - \omega_{kj}|}{\omega_i} \times 100\%. \tag{14}$$

In this work the tolerance ε was set to 10%, which means that the single stage mode must be within 10% of the multi-stage mode in order for the modal alignment to be tested.

Using the information from Eqns. 11, 12 and 13, six types of modes are possible. Essentially, the energy ratio is used to classify the dominance of the mode as stage 1, stage 2, or multi-stage. Then, the MAC number is used to identify if the multi-stage mode is actually aligned with a corresponding single stage mode. A summary of these mode types is given in Tab. 1.

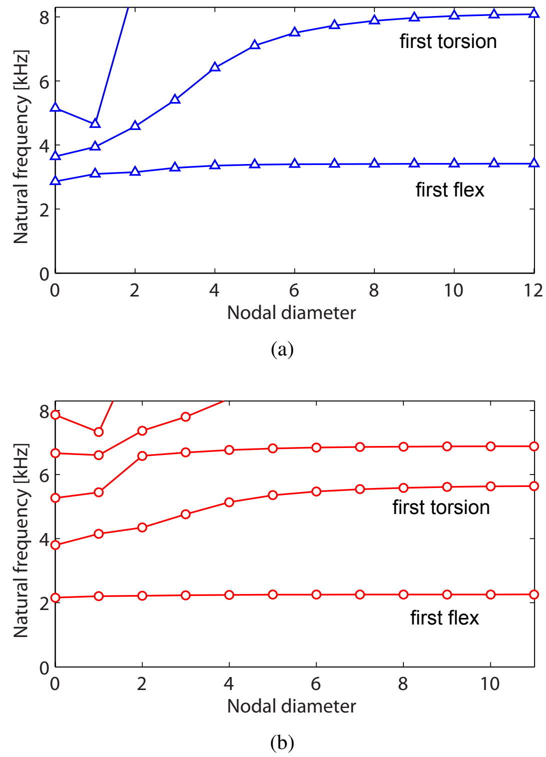

FIGURE 3. NODAL DIAMETER VERSUS FREQUENCY PLOTS FOR (a) STAGE 1 AND (b) STAGE 2.

ANALYSIS

Many ROMs were created using the methodology presented in the *Multi-Stage ROMs from Cyclic Stages* section herein. The system analyzed is a two stage rotor shown in Fig. 2. The first stage of the blisk contains 25 identical blades and the second stage contains 23 blades. Single stage analyses were conducted on each stage to obtain the frequency versus nodal diameter plots shown in Fig. 3. In the frequency range 0 – 8 kHz, there are two mode families for stage 1, and three mode families for stage 2.

The FEM of the multi-stage system contains 136,488 DOFs, while each of the ROMs contains only 592 DOFs (0.5% of the original FE size). Each ROM uses 23 Fourier basis functions to model the dynamics at the interface between stages. Note that the full multi-stage FEM never needs to be assembled to create the ROMs in this work, it is only constructed for validation purposes. The ROMs were created from 1,000 different mistuning patterns applied to each stage with 20 different mistuning levels with standard deviations ranging from 0% to 10%. While the ROMs were developed to be valid (with respect to the full FEM) over a frequency range of 0 – 20 kHz, the results below are focused on a narrower frequency range of 0 – 8 kHz. One mistuned ROM with a 4% standard deviation mistuning level was validated

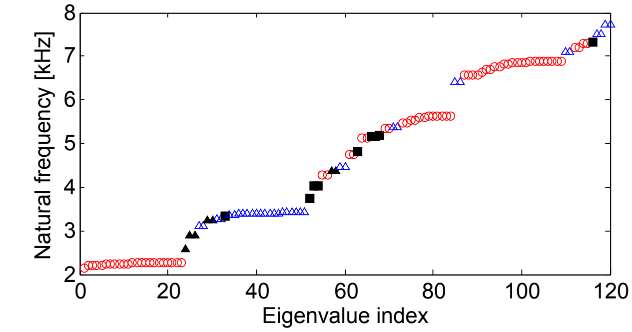

(a)

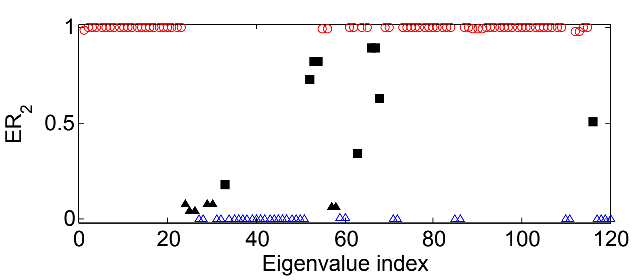

(b)

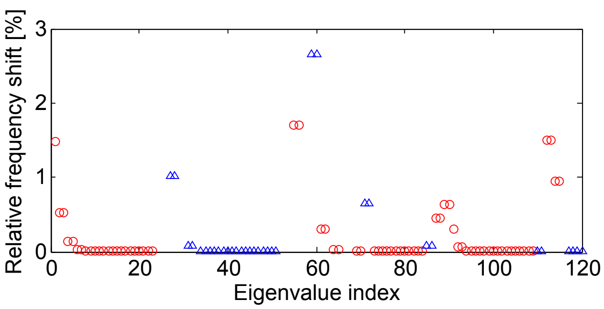

(c)

FIGURE 4. (a) FREQUENCIES OF THE TUNED MULTISTAGE SYSTEM, (b) ENERGY RATIO IN THE CORRESPONDING MODES, AND (c) RELATIVE FREQUENCY DIFFERENCE BETWEEN THE MULTI-STAGE SYSTEM AND THE SINGLE STAGE SYSTEM MODES.

with respect to the FEM. The relative error of the ROM frequencies with respect to the FEM for the first 200 modes was less than 0.05%. Additionally, forced response calculations were carried out in the multi-stage frequency regime 2.8 – 3.4 kHz. The error at the peak responses was approximately 1% on both stages.

The first set of multi-stage results obtained is a classification of the tuned system modes of the multi-stage system using the criteria given in Tab. 1. The results are summarized in Fig. 4 for the first 120 modes. For Fig. 4(a), the x-axis is the eigenvalue index, while the y-axis is the multi-stage natural frequency. For

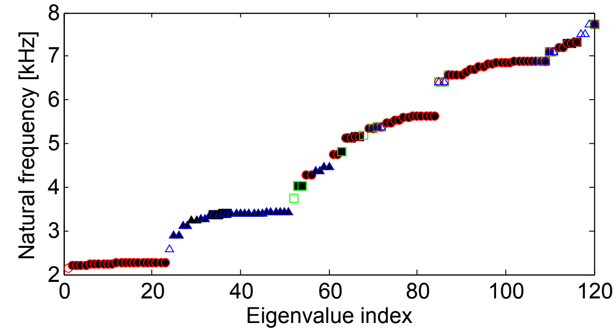

(a)

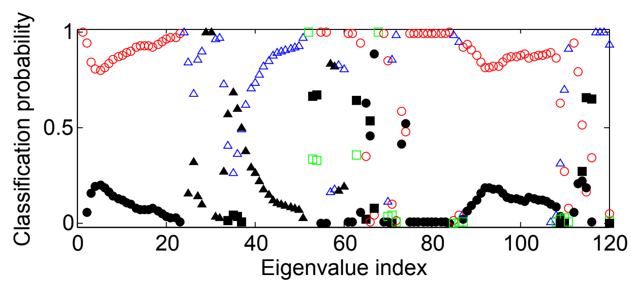

(b)

FIGURE 5. (a) FREQUENCIES OF THE MISTUNED MULTI-STAGE SYSTEM AND (b) THE PROBABILITY OF THE CLASSIFICATION OF THE CORRESPONDING MODES.

Fig. 4(b), the x-axis is the eigenvalue index, while the y-axis is the energy ratio in stage 2 ER_2 (a value of 1 indicates that the energy is contained entirely in stage 2, while a value of 0 indicates that the energy is contained entirely in stage 1). For Fig. 4(c), the x-axis is again the eigenvalue index, while the y-axis is the relative frequency difference between modes computed for the multi-stage system and the corresponding modes computed for a single stage system. Note that for all multi-stage modes (M_{S1}, M_{S2} and $M_{1,2}$), no value is plotted because there is no single stage mode to compare with these multi-stage modes.

It is evident that there are a couple of narrow frequency ranges, e.g. 2 – 2.4 kHz and 6.5 – 7.0 kHz, where stage 2 only models may be used to model the *tuned* system dynamics. Whereas other regions tend to include a mixture of $S1$, $S2$, M_{S1}, and $M_{1,2}$ modes, which means that *these regions require a multi-stage analysis* to be valid.

Next we examine the effects of mistuning. Consider the mistuned results for 1,000 distinct mistuning patterns with a standard deviation of the mistuning of 5%. The results are presented in Fig. 5(a) with the same layout as in Fig. 4(a), with the tuned frequencies once again being plotted. All classification symbols are plotted for each index if that classification occurs for at least one mistuning pattern. In Fig. 5(b), the corresponding probability for each classification at each eigenvalue index is plotted.

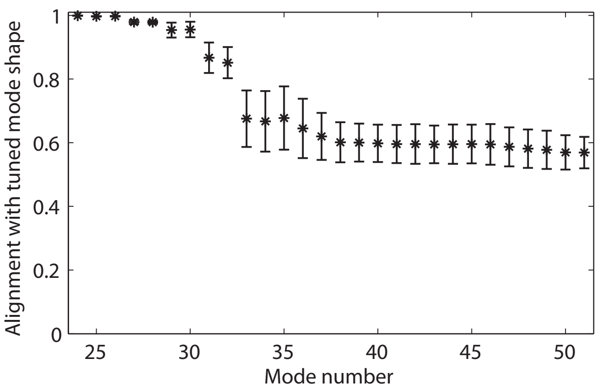

FIGURE 6. ALIGNMENT OF MISTUNED MULTI-STAGE MODES WITH TUNED MULTI-STAGE MODES.

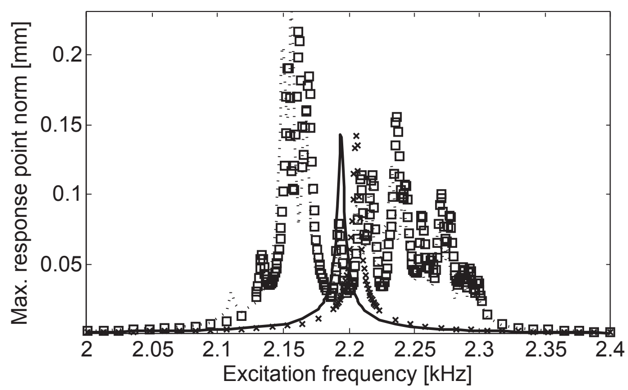

FIGURE 7. FORCED RESPONSE OF STAGE 2 FOR A SET OF STAGE 2 DOMINATED MODES, WHICH ARE $S2$ WHEN TUNED AND M_{S2} WHEN MISTUNED (TUNED SINGLE STAGE ANALYSIS [x], TUNED MULTI-STAGE ANALYSIS [-], MISTUNED SINGLE STAGE ANALYSIS [□], AND MISTUNED MULTI-STAGE ANALYSIS [...]).

This figure shows the very complex interactions and possibilities that exist when dealing with statistical distributions of mistuning patterns in multi-stage systems. For example, consider the narrow frequency ranges 2 – 2.4 kHz and 6.5 – 7.0 kHz where single stage analyses can be used for the *tuned* system. For mistuned systems, in these ranges there is approximately a 20% chance that some of the modes are multi-stage M_{S2} modes. Outside of those narrow frequency ranges even more complex interactions occur which lead to a probability of the creation M_{S1}, M_{S2}, $M_{S1,S2}$, and $M_{1,2}$ modes.

To investigate the effects of mistuning on the multi-stage system, the alignment of each mistuned multi-stage mode with its corresponding tuned multi-stage mode was also calculated. The results for the modes in the frequency range 2.5 – 3.5 kHz are plotted in Fig. 6. The mistuning level was 5% and 1,000 different mistuning patterns were simulated. Average alignments and standard deviation bars are plotted in Fig. 6. The alignment is calculated in the reduced space between mass normalized tuned and mistuned eigenvectors using the MAC number. One can observe that the more isolated modes (23 – 27) have a much greater mistuned-tuned alignment than the rest of the modes in this mode family. That is consistent with the intuitive observation that the mistuned modes in the flat region of a mode family can change shape (compared to their tuned versions) more than other modes.

To better understand the results presented in Fig. 4 and Fig. 5, forced response calculations were conducted. A structural damping of the form $j\gamma\mathbf{K}$ was used, where $j = \sqrt{-1}$, $\gamma = 0.002$, and $\mathbf{K}$ is the stiffness matrix. Also, forces were applied at the tip of the blades with specified engine order excitations, and the maximum response of the excited nodes was collected as the maximum forced response. These tip nodes were used for the forced response because the dominant motion on both stages is due to the first flexural modes (see Fig. 3 and Fig. 4) from both stages for the range of frequencies investigated. First an engine order 1 excitation was applied at 512 evenly sampled frequencies from 2 kHz to 2.4 kHz. The y-axis of the plot corresponds to the maximum response of the excited nodes. Figure 7 shows the forced response of stage 2 for four cases. The first case is when a single stage analysis is conducted on the tuned stage 2. The second case is when a multi-stage analysis is conducted on the tuned multi-stage system. The third case is when a single stage analysis is conducted on a mistuned stage 2. The final case is a multi-stage analysis of the mistuned multi-stage system. The tuned single and tuned multi-stage results have a very similar magnitude with just a shift in frequency location, which agrees with the results presented in Fig. 4 (which shows that the MAC is greater than 0.9 over the entire frequency range). Note, due to the difference in frequency between the single and the multi-stage modes (shown in Fig. 4(c)), a slight shift in frequency for the largest responses is to be expected. The mistuned single stage and multi-stage analyses do not match as well as the tuned analyses. They contain significant differences in amplitude and location of peaks. This agrees with Fig. 5 since a mistuning pattern was chosen which would have at least one M_{S2} mode in the frequency range of interest. This means that at least one MAC number is less than 0.9 in the frequency range of interest, and therefore the single stage modes are no longer aligned with the modes of the multi-stage system over this frequency range. Additionally, the results for stage 1 are not plotted since for all four cases the amplitude of vibration is very low, which is to be expected because $ER_1 < 0.1$ for all modes in the frequency range for all four cases. This highlights that a mode of a multi-stage system can be energetically contained to a single stage and yet may still be significantly different than a single stage mode. Hence,

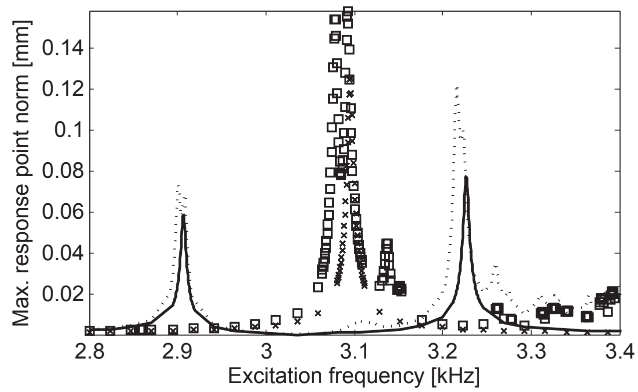

(a)

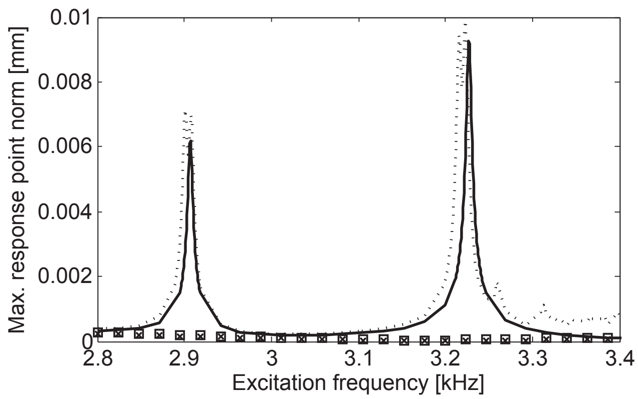

(b)

FIGURE 8. FORCED RESPONSE FOR A SET OF $S1$, M_{S1}, AND $M_{1,2}$ MODES FOR (a) STAGE 1 AND (b) STAGE 2 (TUNED SINGLE STAGE ANALYSIS [x], TUNED MULTI-STAGE ANALYSIS [-], MISTUNED SINGLE STAGE ANALYSIS [□], AND MISTUNED MULTI-STAGE ANALYSIS [. . .]).

multi-stage calculations must be performed to accurately predict the response of such systems.

Forced response simulations were also conducted at 1,024 evenly spaced points from 2.8 – 3.4 kHz using an engine order 1 excitation. As can be seen from Fig. 4 and Fig. 5 the modes in this frequency range are characterized as stage 1 dominated modes ($S1$ and M_{S1}) and multi-stage modes ($M_{1,2}$). The results for these simulations are presented in Fig. 8 (and the four cases are the same as the ones presented in Fig. 7). Due to important multi-stage effects there is a significant response in both stages. The single stage analyses (tuned and mistuned) cannot capture these multi-stage effects. In Fig. 8(b), the single stage analyses (both tuned and mistuned) predict almost no motion over this frequency range, but the multi-stage analyses (both tuned and mistuned) show that there is considerable motion. In Fig. 8(a),

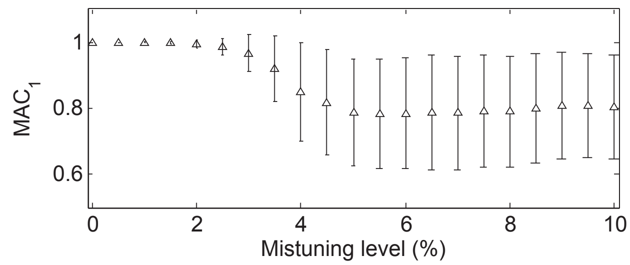

(a)

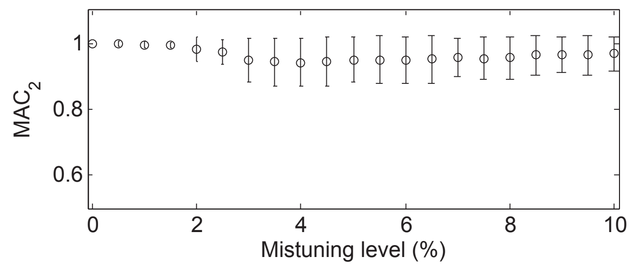

(b)

FIGURE 9. MAC NUMBER VERSUS MISTUNING LEVEL FOR (a) MODE 36 [$S1$, M_{S1}] AND (b) MODE 6 [$S2$, M_{S2}] (ERROR BARS INDICATE THE STANDARD DEVIATION OF THESE VALUES FOR 100 MISTUNING PATTERNS).

there is motion predicted by the single stage analyses (which is to be expected since single stage dominated modes are present), but the magnitude and frequency are not accurate. Hence, multi-stage calculations are certainly required.

The results in Fig. 8 indicate when the multi-stage analyses (versus single stage analyses) are of primary importance for both tuned and mistuned systems. In contrast, Fig. 7 shows that single stage analyses are valid for tuned systems (with just a slight frequency shift). However, single stage analyses are not valid for arbitrary mistuned systems. To predict the validity of single stage versus multi-stage and tuned versus mistuned analyses one must use Figs. 4 and 5.

A key parameter that affects both the classification of modes and the forced response of the system is the level of mistuning. Figure 9 explores the effect of the mistuning level on the multi-stage mode classification. Figure 9(a) is a plot of MAC_1 versus mistuning level for mode 36 (a stage 1 dominated mode) for 100 mistuning patterns with average and standard deviation bars plotted. Figure 9(b) is a plot of MAC_2 versus mistuning level for mode 6 (a stage 2 dominated mode) for 100 mistuning patterns with average and standard deviation bars plotted. The deviations for mode 36 are larger than for mode 6, which is to be expected since (from Fig. 5(b)) mode 36 has a 60% chance of changing from $S1$ to M_{S1} at a 5% mistuning level, whereas mode 6 has only an 18% chance of changing from $S2$ to M_{S2}. Also, as expected,

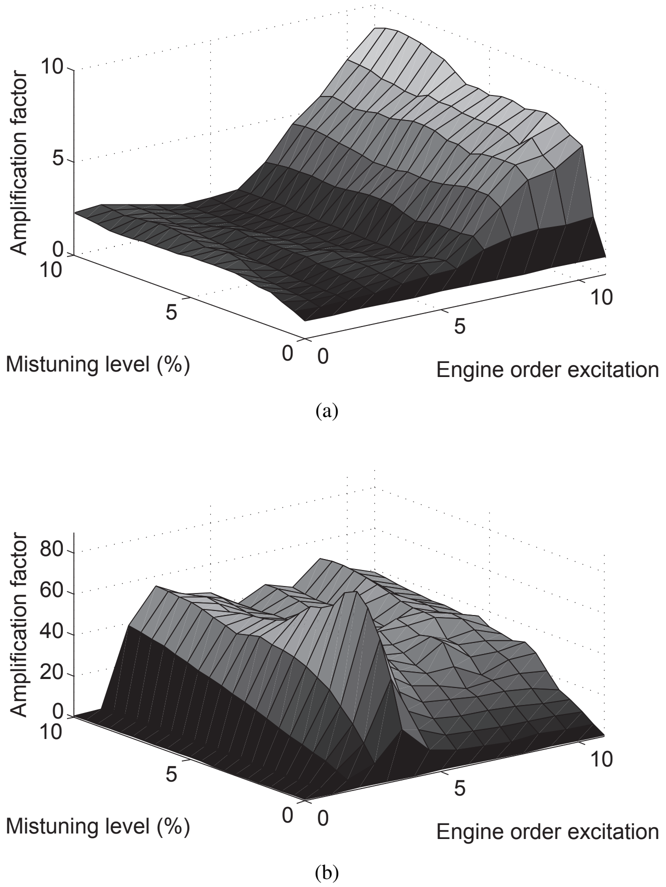

FIGURE 10. FORCE AMPLIFICATION FACTOR VERSUS MISTUNING LEVEL AND ENGINE ORDER EXCITATION FOR THE MULTI-STAGE SYSTEM FOR (a) STAGE 1 AND (b) STAGE 2.

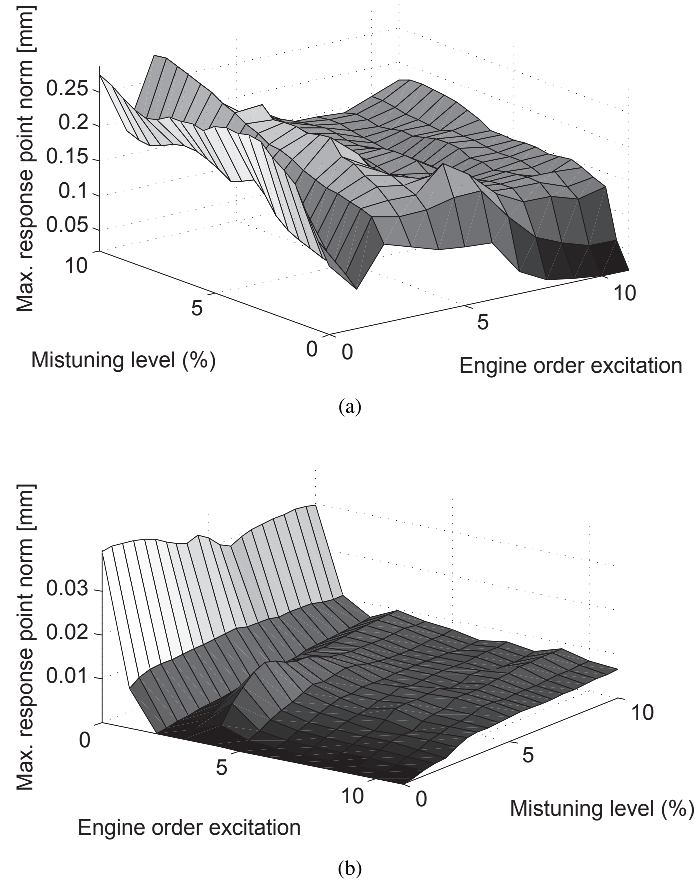

FIGURE 11. MAXIMUM FORCE RESPONSE VERSUS MISTUNING LEVEL AND ENGINE ORDER EXCIATION FOR THE MULTI-STAGE SYSTEM FOR (a) STAGE 1 AND (b) STAGE 2.

initially the deviations in the MAC number for both modes increases while the actual average MAC number decreases as the mistuning level increases. However, it is interesting to note that the average MAC numbers and the deviations in the MAC number level off at around 4 – 5% standard deviation in the mistuning level.

Figure 10 contains amplification factor plots for stage 1 and 2 of the 99$^{\text{th}}$ percentile response of 100 mistuning patterns for engine order excitation 0 to 11 and mistuning levels from 0% to 10% over the frequency range 2.8 – 3.4 kHz. One hundred separate forced response calculations were performed at each unique mistuning level and engine order excitation combination. In this case, the amplification factor for each stage is defined as the number that when multipled by the tuned response at a given engine order excitation would give the 99$^{\text{th}}$ percentile maximum response for this set of mistuning patterns.

The results in Fig. 10 show that stage 2 has a much larger amplification factor than stage 1. This does not mean that the response of stage 2 is larger, in fact it is an order of magnitude lower. The actual 99$^{\text{th}}$ percentile response for these mistuning patterns for stage 1 and 2 are shown in Fig. 11. Note that the motion at lower engine order excitations is larger than at higher engine order excitations. This is likely due to the the multi-stage region moving from one family of stage 2 dominated modes to stage 1 dominated modes (see Figs. 3 and 4). This region relates to nodal diameters 0, 1 and 2 (of stage 1) and also corresponds to a kind of veering region where blade and disk motion are coupled, which leads to larger responses.

DISCUSSION AND CONCLUSIONS

A novel methodology was used to generate multi-stage reduced order models (ROMs) that requires only single sector full order models. This efficient methodology reduces the individual stages using a combination of component mode synthesis, component mode mistuning and cyclic symmetry analysis. The synthesis of the multi-stage ROM was completed in the reduced coordinates by projecting the motion along the interface between stages onto a set of harmonic basis functions and then enforcing geometric compatibility. The methodology was applied to a two stage system to create a variety of ROMs and conduct statistical analyses. Additionally, a new classification scheme was developed for categorizing modes of multi-stage bladed disk systems. The classification scheme is based on sorting modes based on the energy distribution between the stages and the alignment of modes of the multi-stage system with modes from single stage systems.

Several conclusions can be drawn from this work. First, narrow frequency ranges can exist where single stage analyses are valid for *tuned* multi-stage systems. However, when considering mistuning, the modes in these frequency ranges often no longer match their single stage counterparts, thus significantly changing the forced response predictions although the energy does remain contained to the corresponding single stage. Additionally, outside of these narrow frequency ranges, multi-stage analyses are always required because multi-stage modes exist and therefore, a single stage analysis will be very inaccurate. Mistuning in multi-stage systems creates even more complex dynamics that need to be analyzed in a probabilistic manner. Therefore, many mistuning patterns need to be generated and efficient ROMs for performing calculations for the multi-stage system are critical. Also, it was observed that as the mistuning level is increased it has an increasing impact (increasing the amplification factor and decreasing the modal alignment). However, the influence levels off at approximately 5% standard deviation in the mistuning level for the two stage blisk investigated in this work.

ACKNOWLEDGMENT

The partial financial support of the Air Force Office of Scientific Research through grant FA9550-08-1-0276 (Dr. Douglas Smith, Program Manager) is gratefully acknowledged.

REFERENCES

[1] Castanier, M. P., and Pierre, C., 2006. "Modeling and analysis of mistuned bladed disk vibration: Status and emerging directions". *Journal of Propulsion and Power,* ***22***, March, pp. 384–396.

[2] Ewins, D. J., 1969. "The effects of detuning upon the forced vibrations of bladed disks". *Journal of Sound and Vibration,* ***9***(1), pp. 65–79.

[3] Dye, R. C. F., and Henry, T. A., 1969. "Vibration amplitudes of compressor blades resulting from scatter in blade natural frequencies". *ASME Journal of Engineering for Power,* ***91***(3), pp. 182–188.

[4] Griffin, J. H., and Hoosac, T. M., 1984. "Model development and statistical investigation of turbine blade mistuning". *ASME Journal of Vibration , Acoustics, Stress, and Reliability in Design,* ***106***(2), pp. 204–210.

[5] Wei, S.-T., and Pierre, C., 1988. "Localization phenomena in mistuned assemblies with cyclic symmetry Part I: Free vibrations". *ASME Journal of Vibration, Acoustics, Stress, and Reliability in Design,* ***110***, pp. 429–438.

[6] Wei, S.-T., and Pierre, C., 1988. "Localization phenomena in mistuned assemblies with cyclic symmetry Part II: Forced vibrations". *ASME Journal of Vibration, Acoustics, Stress, and Reliability in Design,* ***110***, pp. 439–449.

[7] Hurty, W. C., 1965. "Dynamic analysis of structural systems using component modes". *AIAA Journal,* ***3***(4), pp. 678–685.

[8] Craig, R. R., and Bampton, M. C. C., 1968. "Coupling of substructures for dynamic analyses". *AIAA Journal,* ***6***(7), pp. 1313–1319.

[9] Craig, R. R., and Chang, C.-J., 1976. "Free-interface methods of substructure coupling for dynamic analysis". *AIAA Journal,* ***14***(11), pp. 1633–1635.

[10] Irretier, H., 1983. "Spectral analysis of mistuned bladed disk assemblies by component mode synthesis". In *Vibrations of Bladed Disk Assemblies*, D. J. Ewins and A. V. Srinivasan, eds. American Society of Mechanical Engineers, New York, pp. 115–125.

[11] Zheng, Z.-C., and Wang, F.-R., 1985. "Dynamic analysis of blade groups using component mode synthesis". In *Vibrations of Blades and Bladed Disk Assemblies*, R. E. Kielb and N. F. Rieger, eds. American Society of Mechanical Engineers, New York, pp. 97–103.

[12] Yang, M. T., and Griffin, J. H., 2001. "A reduced-order model of mistuning using a subset of nominal system modes". *Journal of Engineering for Gas Turbines and Power - Transactions of the ASME,* ***123***, Oct., pp. 893–900.

[13] Lim, S.-H., Bladh, R., Castanier, M. P., and Pierre, C., 2007. "Compact, generalized component mode mistuning representation for modeling bladed disk vibration". *AIAA Journal,* ***45***(9), pp. 2285–2298.

[14] Sinha, A., 2008. "Reduced-order model of a mistuned multi-stage bladed rotor". *International Journal of Turbo and Jet Engines,* ***25***(3), pp. 145–153.

[15] Bladh, R., Castanier, M. P., and Pierre, C., 2003. "Effects of multistage coupling and disk flexibility on mistuned bladed disk dynamics". *Journal of Engineering for Gas Turbines and Power - Transactions of the ASME,* ***125***(1), pp. 121–130.

[16] Song, S. H., Castanier, M. P., and Pierre, C., 2005. "Multi-stage modeling of turbine engine rotor vibration". In Proceedings of the ASME 2005 Design Engineering Technical Conference and Computers and Information in Engineering

Conference. DETC2005-85740.
[17] Song, S. H., Castanier, M. P., and Pierre, C., 2005. "Multi-stage modeling of mistuned turbine engine rotor vibration". In Proceedings of the NATO AVT-121 Symposium on Evaluation, Control and Prevention of High Cycle Fatigue in Gas Turbine Engines for Land, Sea, and Air. RTO-MP-AVT-121-P-06.
[18] Song, S. H., Castanier, M. P., and Pierre, C., 2007. "System identification of multistage turbine engine rotors". In Proceedings of GT2007 ASME Turbo Expo. GT2007-28307.
[19] Song, S. H., 2007. "Vibration analysis and system identification of mistuned multistage turbine engine rotors". PhD thesis, The University of Michigan.
[20] Laxalde, D., Thouverez, F., and Lombard, J.-P., 2007. "Dynamical analysis of multi-stage cyclic structures". *Mechanics Research Communications,* ***34***(4), pp. 379–384.
[21] Laxalde, D., Lombard, J.-P., and Thouverez, F., 2007. "Dynamics of multistage bladed disks systems". *Journal of Engineering for Gas Turbines and Power,* ***129***(4), pp. 1058–1064.
[22] Chatelet, E., D'Ambrosio, F., and Jacquet-Richardet, G., 2005. "Toward global modeling approaches for dynamic analyses of rotating assemblies of turbomachines". *Journal of Sound and Vibration,* ***282***(1-2), pp. 163–178.
[23] Turhan, O., and Bulut, G., 2006. "Linearly coupled shaft-torsional and blade-bending vibrations in multi-stage rotor-blade systems". *Journal of Sound and Vibration,* ***296***(1-2), pp. 292–318.
[24] Rzadkowski, R., and Sokolowski, J., 2005. "Coupling effects between the shaft and two bladed-discs". *Advances in Vibration Engineering,* ***4***(3), pp. 249–266.
[25] Rzadkowski, R., and Drewczynski, M., 2009. "Coupling of vibration of several bladed discs on the shaft, Part I: Free vibration analysis". *Advances in Vibration Engineering,* ***8***(2), pp. 125–137.
[26] Seguì, B., and Casanova, E., 2007. "Application of a reduced order modeling technique for mistuned bladed disk-shaft assemblies". In Proceedings of GT2007 ASME Turbo Expo. GT2007-27594.
[27] D'Souza, K., Saito, A., and Epureanu, B. I., 2010. "Reduced-order-modeling for nonlinear analysis of cracked mistuned multi-stage bladed disk systems". *AIAA Journal,* ***submitted***.
[28] Bladh, R., 2001. *Efficient Predictions of the Vibratory Response of Mistuned Bladed Disks by Reduced Order Modeling,* PhD Thesis. Mechanical Engineering Department, University of Michigan.
[29] Bladh, R., Castanier, M. P., and Pierre, C., 2001. "Component-mode-based reduced order modeling techniques for mistuned bladed disks - Part I: Theoretical models". *Journal of Engineering for Gas Turbines and Power - Transactions of the ASME,* ***123***(1), pp. 89–99.

